Mathematics and Computers in Simulation XXIII (1981) 344–353
North-Holland Publishing Company

PROPAGATION THROUGH NUMERICAL MESH REFINEMENT FOR HYPERBOLIC EQUATIONS

R. VICHNEVETSKY
Department of Computer Science, Rutgers University, New Brunswick, NJ 08903, U.S.A.

1. Introduction

We analyse in this paper *spurious reflection* phenomena that occur at the interface between coarse and fine mesh in the numerical approximation of hyperbolic equations with finite difference methods. The principal tool used is a description of propagation properties of numerical solutions by means of their time-Fourier transforms. The corresponding mathematics are given in the companion paper [1] with which the reader should be familiar.

In Section 3, it is shown that the standard finite difference treatment of the interface point results in conservation of the energy of the numerical solution. Thus (Section 7), the analytic expression of reflection is shown to be also that which ensures continuity of energy flows through the mesh interface.

In Section 4, an exact, analytic expression of reflection at the interface for the standard finite difference treatment is derived. It is given as an integral in the frequency domain, where a reflection ratio function is defined.

In Section 8, we show that the global convergence rate is $O(h^2)$, in spite of the fact that the truncation error at the interface point is only $O(h)$.

In Section 9 we examine in the same vein a modified treatment of the interface that was first proposed in a paper by Browning, Kreiss and Oliger. While the amplitude of reflected solutions for this modified scheme converge to zero as $O(h^3)$, the global accuracy of the calculation is $O(h^2)$ as in the standard case.

2. Standard finite difference approximation in mesh refinement

Consider the simple advection equation

$$\frac{\partial U}{\partial t} + c\frac{\partial U}{\partial x} = 0 \tag{1}$$

on the entire real axis $-\infty < x < \infty$ approximated numerically over two mesh sizes (Fig. 1)

$x_n = nh$, $n = -1, -2, \ldots$,

to the left of the origin, and

$x_n = nk$, $n = 1, 2, \ldots$,

to the right.

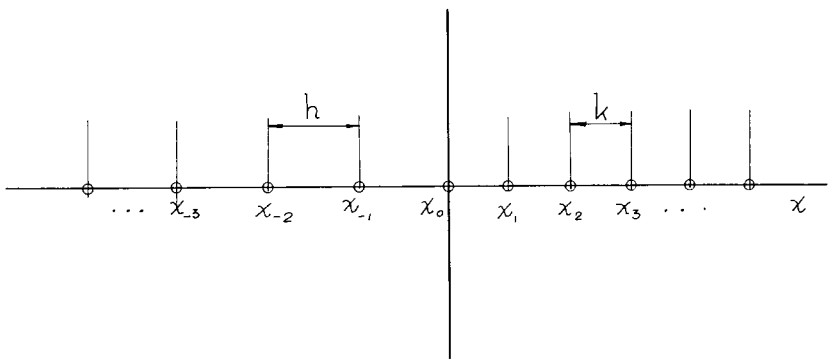

Fig. 1.

0378-4754/81/0000–0000/$02.75

When $k < h$ the situation is described as mesh *refinement*, and when $k > h$ as mesh *coarsening*. Both cases are covered by the analysis.

We wish to analyse the propagation of numerical solutions, in particular as they cross the interface point $x = 0$. The numerical model that we propose to use for this analysis is the simple semi-discretization

$$\frac{du_n}{dt} = -c\left(\frac{u_{n+1} - u_{n-1}}{2h}\right) \quad \text{for } n = -1, -2, \ldots , \tag{2}$$

$$\frac{du_n}{dt} = -c\left(\frac{u_{n+1} - u_{n-1}}{2k}\right) \quad \text{for } n = 1, 2, \ldots \tag{3}$$

and, at the interface point

$$\frac{du_0}{dt} = -c\left(\frac{u_1 - u_{-1}}{h + k}\right). \tag{4}$$

We refer to (4) as the standard treatment of the interface. A modified approximation is described and analysed in Section 9.

This model problem is intended to allow for an analysis of some of the spurious phenomena that occur when nested grids are used in the numerical approximation of hyperbolic equations, such as is found for instance in certain fluid dynamics and atmospheric simulations.

3. Energy

It is well known that the energy of solutions of the advection equation is conserved:

$$\| U(x, t)\|_2^2 \equiv \int_{-\infty}^{\infty} |U(x, t)|^2 \, dx = \text{constant} . \tag{5}$$

(We assume here and in the sequel that U is in $\mathcal{L}_2$, i.e. that $\| U\|_2^2$ is finite.)

The discrete energy of numerical solutions $\{u_n\}$ is defined as

$$\| u_n\|_2^2 \equiv h \sum_{n<0} u_n^2 + \left(\frac{h + k}{2}\right) u_0^2 + k \sum_{n>0} u_n^2 \tag{6}$$

which may be observed to be a rectangular rule approximation of the integral (5).

Numerical solutions of the semi-discretization (2)–(3)–(4) also have constant energy (the semi-discretization is *energy-conservative*). Indeed, the derivative of (6) with respect to time is

$$\frac{d\| u_n\|_2^2}{dt} = 2h \sum_{n<0} u_n \frac{du_n}{dt} + (h + k) u_0 \frac{du_0}{dt} + 2k \sum_{n>0} u_n \frac{du_n}{dt} . \tag{7}$$

Inserting (2), (3) and (4) here results in

$$\frac{d\| u_n\|_2^2}{dt} = [-c u_n u_{n+1}]_{-\infty}^{\infty} \tag{8}$$

which vanishes for solutions that are in $\mathcal{L}_2$.

Thus, (4) may be called an energy conservative approximation of the advection equation over the interface point $x = 0$. (The improved treatment of the interface considered in Section 9 below shall be shown, by contrast, not to conserve energy.)

4. Propagation of numerical solutions

We recall briefly those propagation properties of numerical solutions that shall be used later on (their derivation is given in [1]):

The time Fourier transform of $u_n(t)$ is defined as

$$\hat{u}_n(\Omega) = \int_{-\infty}^{\infty} u_n(t) \, e^{-i\Omega t} \, dt . \tag{9}$$

If the set of functions of time $\{u_n(t)\}$ is a solution of (2), then it may be decomposed as the sum of two *fundamental* solutions:

$$\{u_n(t)\} = \{p_n(t)\} + \{q_n(t)\} \tag{10}$$

which describe those Fourier components in $\{u_n\}$ that carry energy *forward* and *backward*, respectively.

The Fourier transforms of $\{p_n\}$ obey

$$\frac{\hat{p}_{n+1}(\Omega)}{\hat{p}_n(\Omega)} = \hat{E}_1(\Omega) = -i\left(\frac{\Omega h}{c}\right) + \sqrt{1 - \left(\frac{\Omega h}{c}\right)^2} . \tag{11}$$

They have the positive phase velocity

$$c_1^*(\Omega) = \Omega h / \text{arc sin}(\Omega h / c) \tag{12}$$

and the *positive* group velocity

$$\mathcal{V}_1(\Omega) = c\sqrt{1 - \left(\frac{\Omega h}{c}\right)^2} . \tag{13}$$

By contrast, the Fourier transforms of $\{q_n\}$ obey

$$\frac{\hat{q}_{n+1}(\Omega)}{\hat{q}_n(\Omega)} = \hat{E}_2(\Omega) = -i\left(\frac{\Omega h}{c}\right) - \sqrt{1 - \left(\frac{\Omega h}{c}\right)^2}. \quad (14)$$

They have the positive phase velocity

$$c_2^*(\Omega) = \Omega h/(\pi - \arcsin(\Omega h/c)) \quad (15)$$

and the *negative* group velocity

$$\mathcal{V}_2(\Omega) = -c\sqrt{1 - \left(\frac{\Omega h}{c}\right)^2}. \quad (16)$$

Identical properties apply to solutions of (3) in $x > 0$, with k replacing h.

Consider now the propagation through the point $x = 0$ of a solution characterized in that point by the t-Fourier transform:

$$\hat{u}_0(\Omega). \quad (17)$$

To this numerical solution correspond potentially 4 fundamental solutions present near $x = 0$. These are the forward and backward solutions in $x < 0$, and the forward and backward solutions in $x > 0$, respectively.

Since no reflection occurs for large x, only the first three of these fundamental solutions can exist (Fig. 2).

Let $\hat{p}_0, \hat{q}_0$ and $\hat{r}_0$ denote the corresponding Fourier transforms. The equation

$$\hat{p}_0(\Omega) + \hat{q}_0(\Omega) = \hat{u}_0(\Omega) = \hat{r}_0(\Omega) \quad (18)$$

expresses the unicity of u in $x = 0$.

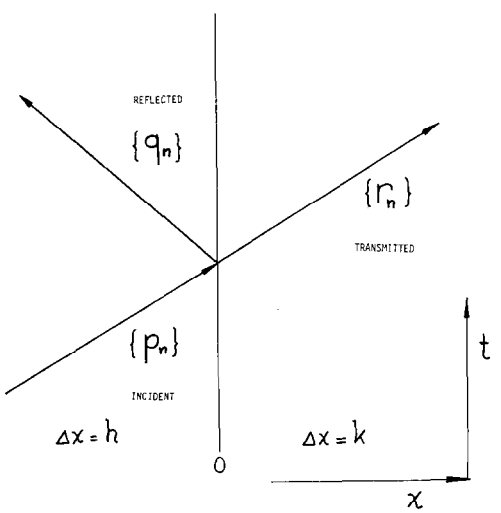

Fig. 2.

Let $\hat{E}_1, \hat{E}_2$ and $\hat{F}_1$ be the characteristic ratios corresponding to $\{p_n\}$, $\{q_n\}$ and $\{r_n\}$, respectively.

That is, numerical solutions are described by (11) and (14) to the left of the origin, and by

$$\frac{\hat{r}_{n+1}(\Omega)}{\hat{r}_n(\Omega)} = \hat{F}(\Omega) = -i\left(\frac{\Omega k}{c}\right) + \sqrt{1 - \left(\frac{\Omega k}{c}\right)^2} \quad (19)$$

to the right. We propose to find the ratio $\rho(\Omega) \equiv \hat{q}_0/\hat{p}_0$ which expresses the amount of reflection at the interface. That is

$$\hat{q}_0(\Omega) = \rho(\Omega)\,\hat{p}_0(\Omega) \quad (20)$$

and, from (18)

$$\hat{r}_0(\Omega) = \hat{u}_0(\Omega) = (1 + \rho(\Omega))\,\hat{p}_0(\Omega). \quad (21)$$

We write the expression of $\hat{u}_1$ and $\hat{u}_{-1}$ in terms of $\hat{p}_0$ and $\hat{q}_0$ as

$$\hat{u}_1 = \hat{F}\hat{u}_0 = \hat{F}(\hat{p}_0 + \hat{q}_0) \quad (22)$$

and

$$\hat{u}_{-1} = \hat{E}_1^{-1}\hat{p}_0 + \hat{E}_2^{-1}\hat{q}_0$$

$$= -(\hat{E}_2\hat{p}_0 + \hat{E}_1\hat{q}_0). \quad (23)$$

The differential equation (4) for u_0 has the Fourier transform

$$i\Omega\hat{u}_0 = -c\left(\frac{\hat{u}_1 - \hat{u}_{-1}}{h + k}\right) \quad (24)$$

or, in terms of $\hat{p}_0$ and $\hat{q}_0$

$$i\Omega(\hat{p}_0 + \hat{q}_0) = -c\left(\frac{\hat{F}(\hat{p}_0 + \hat{q}_0) + (\hat{E}_2\hat{p}_0 + \hat{E}_1\hat{q}_0)}{h + k}\right). \quad (25)$$

Solving for the *reflection ratio* $\rho(\Omega)$ we find, all calculations done,

$$\rho(\Omega) \equiv \frac{\hat{q}_0}{\hat{p}_0} = -\frac{i\Omega(h + k) + c(\hat{E}_2 + \hat{F})}{i\Omega(h + k) + c(\hat{E}_1 + \hat{F})}$$

$$= \frac{\sqrt{1 - \left(\frac{\Omega h}{c}\right)^2} - \sqrt{1 - \left(\frac{\Omega k}{c}\right)^2}}{\sqrt{1 - \left(\frac{\Omega h}{c}\right)^2} + \sqrt{1 - \left(\frac{\Omega k}{c}\right)^2}}. \quad (26)$$

This expression for the reflection ratio becomes particularly interesting if we make use of the expression of the group velocities. Then, for $(\Omega h/c) \leqslant 1$ and

$(\Omega k/c) \leqslant 1$,

$$\rho = \frac{\mathcal{V}_L - \mathcal{V}_R}{\mathcal{V}_L + \mathcal{V}_R}, \tag{27}$$

where $\mathcal{V}_L$ and $\mathcal{V}_R$ are the group velocities to the left and to the right of the origin, viz

$$\mathcal{V}_L = c\sqrt{1 - \left(\frac{\Omega h}{c}\right)^2},$$
$$\mathcal{V}_R = c\sqrt{1 - \left(\frac{\Omega k}{c}\right)^2}. \tag{28}$$

We shall see (in Section 7) that (27) is an expression of the continuity of energy flows through $x = 0$.

The variation of ρ with Ω is illustrated in Fig. 3.

5. Total reflection

Total reflection at the interface occurs when $\Omega k/c > 1$. This happens in mesh coarsening $(k > h)$ for those frequencies Ω for which $h/k < \Omega h/c < 1$.

In those cases, numerical solutions in $x > 0$ are of the type illustrated in [7, Fig. 3]. They have a wavelength equal to $4k$, and an amplitude which decays exponentially with x. They do not carry energy into $x > 0$.

While the amplitude of the reflection ratio is unity, ρ itself becomes a complex number, thus introducing a phase shift between $\hat{q}_0$ and $\hat{p}_0$.

Specifically, when $\Omega k/c > 1$ and $\Omega h/c < 1$, then

$$\rho = \frac{\sqrt{1 - (\Omega h/c)^2} - i\sqrt{(\Omega k/c)^2 - 1}}{\sqrt{1 - (\Omega h/c)^2} + i\sqrt{(\Omega k/c)^2 - 1}}. \tag{29}$$

At the lowest limit of the reflected frequencies $(\Omega k/c = 1)$, we have simply $\rho = +1$.

Also of interest is the other extreme case, $k \to \infty$. Then

$$\rho = \lim_{k\to\infty} \frac{\sqrt{1 - (\Omega k/c)^2} - i\sqrt{(\Omega k/c)^2 - 1}}{\sqrt{1 - (\Omega h/c)^2} + i\sqrt{(\Omega k/c)^2 - 1}} = -1. \tag{30}$$

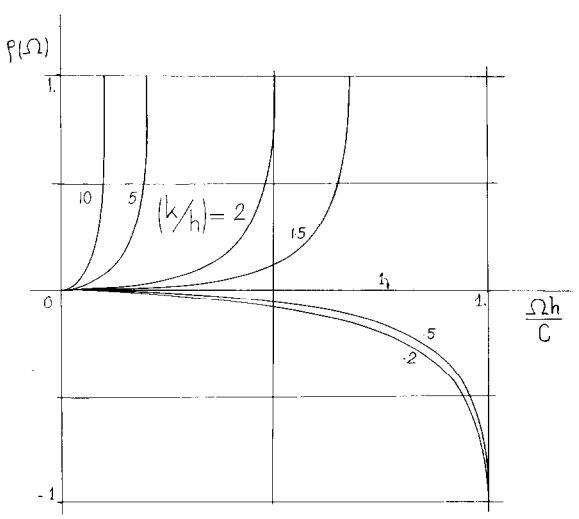

Fig. 3.

6. Passage of a smooth function through the interface

Consider now the passage through the interface point $x = 0$ of a smooth function $\{p_n(t)\}$ with finite support in x. That p is smooth implies that $\{\hat{p}_n(\Omega)\}$ vanishes for values of Ω outside of a narrow band of frequencies:

$$\hat{p}_n(\Omega) = 0 \quad \text{for} \left(\frac{\Omega h}{c}\right) > \gamma; \quad \gamma \ll 1. \tag{31}$$

The expression of the reflected function in $x = 0$ is, from previous results (in particular (20)–(21))

$$q_0(t) = \int \hat{p}_0(\Omega)\, \rho(\Omega)\, e^{i\Omega x}\, \frac{d\Omega}{2\pi} \tag{32}$$

and

$$r_0(t) = p_0(t) + q_0(t)$$
$$= \int \hat{p}_0(\Omega)(1 + \rho(\Omega))\, e^{i\Omega x}\, \frac{d\Omega}{2\pi}. \tag{33}$$

This may also be expressed in terms of x-Fourier transforms. If $\overline{p}(\omega, 0)$ is the discrete x-Fourier transform of $\{p_n(0)\}$, then the Fourier transform of the reflected function $\{q_n(t)\}$ is (after reflection, i.e. for $t >$ some T) of the form

$$|\overline{q}(\omega_q, t)| = \left|\overline{p}\left(\frac{\pi}{h} - \omega_q, 0\right) \rho\left(\frac{\pi}{h} - \omega_q\right)\right| \tag{34}$$

where $|\omega_q|$ is in $[\pi/2h, \pi/h]$.

Since to small values of Ω correspond fundamental solutions of the $\{q_n\}$ type with wavelength near $2h$, it will be the case that the reflected solution will consist mostly of a $2h$-wavelength oscillatory function modu-

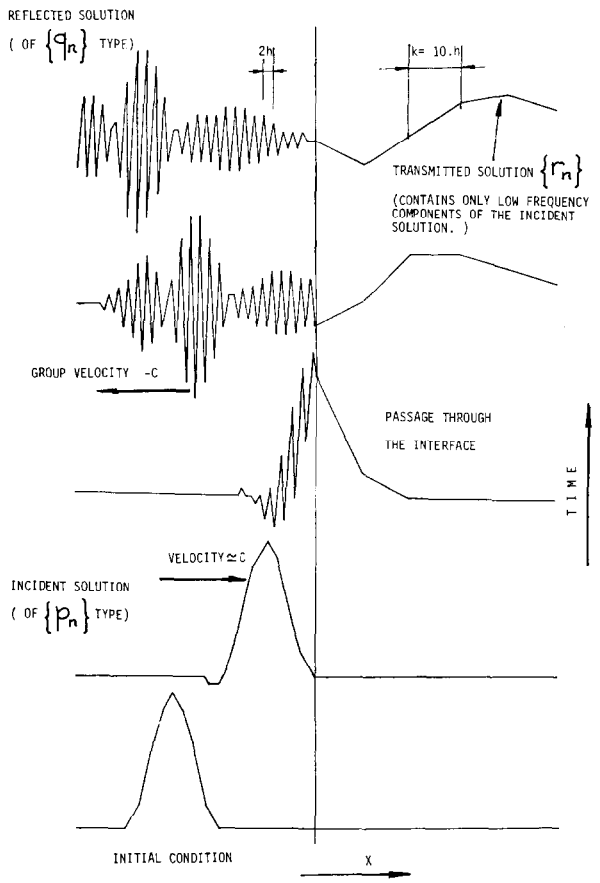

Fig. 4. Passage of a smooth function through the interface point $x = 0$ with $(k/h) > 1$. The reflected solution consists of an almost $(2h)$ wavelength sinusoidal function modulated by a smooth envelope.

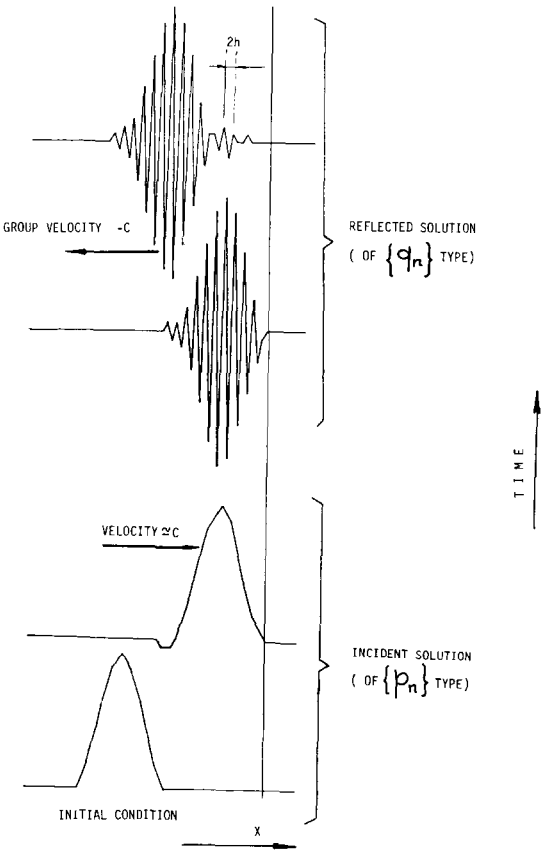

Fig. 5. An illustration of total reflection when $k/h >> 1$.

lated by a smooth envelope whose x-Fourier transform has the amplitude

$$|\overline{p}(-\omega, 0)\, \rho(-\omega)| \,. \tag{35}$$

The energy contained in the reflected solution is given by

$$\|q_n\|_2^2 = \int_{-\pi/2h}^{\pi/2h} |\overline{p}(\omega, 0)\, \rho(\omega)|^2 \, \frac{d\omega}{2\pi} < \|p_n\|_2^2 \,. \tag{36}$$

A numerical example is illustrated in Fig. 4.

When $k >> h$, then, as we have seen, $\rho(\Omega) \simeq -1$ for all frequencies. The reflected solution then consists of a mostly $(2h)$ wavelength oscillatory function.

Since there is no phase distortion at the interface, the envelope of the reflected function is in this case (almost) identical to the incident function. This is illustrated in the numerical example of Fig. 5.

7. Energy conservation

We have seen in Section 3 that the semi-discretization (2)–(3)–(4) is energy conservative. The expression of this property takes here the following form:

Consider the passage through $x = 0$ of the smooth function analyzed in the preceding section. Initially, the energy is contained entirely in $\{p_n\}$ on $x < 0$:

$$\|u_n(0)\|_2^2 = \|p_n(0)\|_2^2 \,. \tag{37}$$

Its passage through the point $x = 0$ is expressed by the equation that describes energy flow. From [1, eq. (74)],

$$\|p_n(0)\|_2^2 = \int_{-c/h}^{c/h} |\hat{p}_0(\Omega)|^2 \mathcal{V}_L(\Omega) \frac{d\Omega}{2\pi} . \quad (38)$$

The energy reflected in $\{q_n\}$ is, likewise

$$\|q_n\|_2^2 = \int_{-c/h}^{c/h} |\rho(\Omega)\, \hat{p}_0(\Omega)|^2 \mathcal{V}_L(\Omega) \frac{d\Omega}{2\pi} \quad (39)$$

and the transmitted energy is

$$\|r_n\|_2^2 = \int_{-c/h}^{c/h} |(1+\rho)\, \hat{p}_0(\Omega)|^2 \mathcal{V}_R(\Omega) \frac{d\Omega}{2\pi} . \quad (40)$$

The sum of the transmitted and the reflected energy is thus

$$\|q_n\|_2^2 + \|r_n\|_2^2 =$$

$$= \int [|\rho\, \hat{p}_0(\Omega)|^2 \mathcal{V}_L + |(1+\rho)\, \hat{p}_0(\Omega)|^2 \mathcal{V}_R] \frac{d\Omega}{d\pi}$$

$$= \int [\rho^2 \mathcal{V}_L + (1+\rho)^2 \mathcal{V}_R] |\hat{p}_0(\Omega)|^2 \frac{d\Omega}{2\pi} . \quad (41)$$

But, using (27), we find that

$$\rho^2 \mathcal{V}_L + (1+\rho)^2 \mathcal{V}_R = \mathcal{V}_L . \quad (42)$$

Thus,

$$\|q_n\|_2^2 + \|r_n\|_2^2 = \mathcal{V}_L |\hat{p}_0(\Omega)|^2 \frac{d\Omega}{2\pi}$$

$$= \|p_n\|_2^2 . \quad (43)$$

This reads: *The incident energy is equal to the sum of the reflected and of the transmitted energy.*

8. Convergence rates

We derive in this section convergence rates for the different components of the solution. We show that in spite of the fact that the truncation error of the discretization equation (4) at the interface is $O(h)$, the global accuracy of the semi-discretization is $O(h^2)$:

Consider a solution of $\{p_n\}$ type that exists at the interface point $x = 0$, and that has been generated for instance by a prescribed boundary condition $U(-l, t)$ at some point $x = -l$ to the left of the origin.

The Fourier transform of the exact solution in $x = 0$ is

$$\hat{U}(0, \Omega) = \hat{U}(-l, \Omega)\, e^{-i\Omega Nh/c} , \quad (44)$$

while that of the forward numerical solution is

$$\hat{p}_0(\Omega) = \hat{U}(-l, \Omega)(\hat{E}_1(\Omega))^N . \quad (45)$$

Here, N, the number of divisions between $x = -l$ and $x = 0$, is

$$N = \frac{l}{h} .$$

The Fourier transform of the corresponding error is thu

$$\hat{e}_0 \equiv \hat{p}_0 - \hat{U}(0, \Omega)$$

$$= \hat{U}(-l, \Omega)[[\hat{E}_1(\Omega)]^N - e^{-i\Omega Nh/c}] , \quad (46)$$

Expanding in Taylor series:

$$\hat{e}_0 = \hat{U}(-l, \Omega)\left[\left(1 - i\frac{\Omega h}{c} - \frac{1}{2}\left(\frac{\Omega h}{c}\right)^2 - \frac{1}{8}\left(\frac{\Omega h}{c}\right)^4 \cdots\right)^N - \left(1 - i\frac{\Omega h}{c} - \frac{1}{2}\left(\frac{\Omega h}{c}\right)^2 + \frac{i}{6}\left(\frac{\Omega h}{c}\right)^3 + \cdots\right)^N\right]$$

$$= \hat{U}(-l, \Omega)\left[\frac{i}{6}\left(\frac{\Omega h}{c}\right)^3 \frac{l}{h} + \cdots\right]$$

$$= O(h^2) \quad (47)$$

gives the order of accuracy of numerical solutions of $\{p_n\}$ type in $x \leqslant 0$:

$$\{p_n\} = \{U(x_n, t)\} + O(h^2) . \quad (48)$$

I.e., $\{p_n\}$ *approximates the exact solution in* $x \leqslant 0$ *with an error that converges to zero as* $O(h^2)$.

This agrees with the fact that the truncation error of (2) expressed in classical form is also of second order in h:

$$T_{h,n} \equiv \left(\frac{\partial U}{\partial t}\right)_n + c\left(\frac{U_{n+1} - U_{n-1}}{2h}\right)$$

$$= \frac{c}{6}\left(\frac{\partial^3 U}{\partial x^3}\right)_n h^2 + \text{higher order terms}$$

$$= O(h^2) . \quad (49)$$

To analyse global convergence, we define a family of calculations in which $h \to 0$ and $k \to 0$ with $h/k \neq 1$ remaining constant.

The reflection ratio may then be expanded as

$$\rho(\Omega) = \frac{\left(1 - \frac{1}{2}\left(\frac{\Omega h}{c}\right)^2 + \cdots\right) - \left(1 - \frac{1}{2}\left(\frac{\Omega k}{c}\right)^2 + \cdots\right)}{2 + \cdots}$$

$$= -\frac{1}{4}\left(\frac{\Omega}{c}\right)^2 (h^2 - k^2) + \cdots$$

$$= O(h^2 - k^2) = O(h^2) . \tag{50}$$

Thus, the amplitude of the reflected solution $\{q_n\}$ after the passage of $\{p_n\}$ through $x = 0$ is also of second order in h, since

$$\hat{q}_0(\Omega) = \hat{p}_0(\Omega)\,\rho(\Omega)$$

$$= \hat{U}(0, \Omega)(1 + O(h^2))\, O(h^2)$$

$$= O(h^2) . \tag{51}$$

From this, it is easy to show that $\{q_n\}$, *which is spurious, converges to zero as* $O(h^2)$.

The error in $\hat{r}_0(\Omega)$ is also $O(h^2)$:

$$\hat{r}_0(\Omega) = \hat{p}_0(\Omega)(1 + \rho(\Omega))$$

$$= p_0(\Omega)(1 + O(h^2))$$

$$= \hat{U}(0, \Omega)(1 + O(h^2)) \tag{52}$$

and, by the same argument than that leading to (48), for finite $n > 0$,

$$\{r_n\} = \{U(x_n, t)\}(1 + O(h^2)) . \tag{53}$$

Or $\{r_n\}$ *approximates the exact solution in* $x > 0$ *with an error that converges to zero as* $O(h^2)$.

Thus, the global rate of convergence of the approximation (2)–(3)–(4) is $O(h^2)$ (see Fig. 6).

We note that this is in spite of the fact that the accuracy of the difference formula at the boundary is only $O(h)$:

$$T_{h,0} \equiv \left(\frac{\partial U}{\partial t}\right)_0 + c\left(\frac{U_1 - U_{-1}}{h + k}\right)$$

$$= \frac{c}{2}\left(\frac{\partial^2 U}{\partial x^2}\right)_0 (k - h) + \cdots$$

$$= O(h) . \tag{54}$$

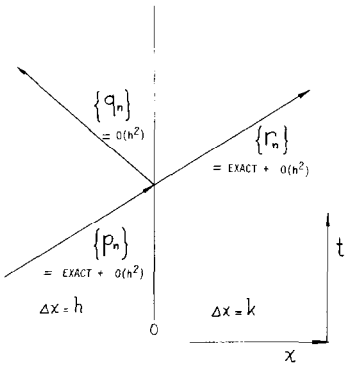

Fig. 6. Convergence rates of the different components of the numerical solution in the 'standard' treatment of the interface point.

This result is not unexpected: it is analogous to the known property that the global rate of convergence of the numerical approximation of a hyperbolic equation is equal to the order of the truncation error in the computational domain even if the truncation error at the boundaries is one order less (see e.g. [5]).

9. A modified treatment of the interface

We now examine a refinement procedure for hyperbolic equations that has been described by Browning, Kreiss and Oliger [2]. Their approach is similar to a procedure used by Isaacson [6] to handle discontinuous coefficients of parabolic equations.

The discrete mesh is chosen as

$$x_n = \begin{cases} (n + \frac{1}{2})\,h & \text{for } n = 0, -1, -2, \ldots , \\ (n - \frac{1}{2})\,k & \text{for } n = 0, 1, 2, \ldots . \end{cases} \tag{55}$$

This creates an overlap of the two meshes in the vicinity of the interface point $x = 0$, as shown in Fig. 7.

The standard finite-difference expressions (2) and (3) are used in $x < 0$ and $x > 0$, respectively. The two solution values near the origin, $u_{0,L}$ and $u_{0,R}$, are computed from the equations that express continuity of u and $\partial u/\partial x$ in $x = 0$, viz.

$$u_{0,L} + u_1 = u_{-1} + u_{0,R} , \tag{56}$$

$$\frac{u_1 - u_{0,L}}{k} = \frac{u_{0,R} - u_{-1}}{h} \tag{57}$$

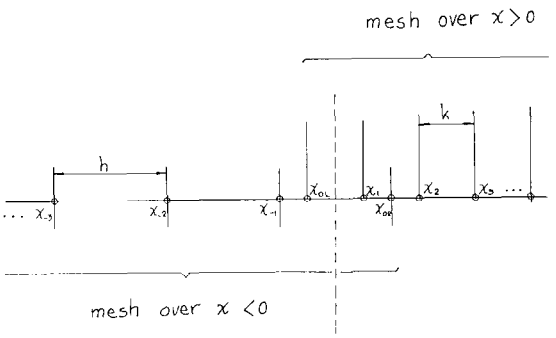

Fig. 7.

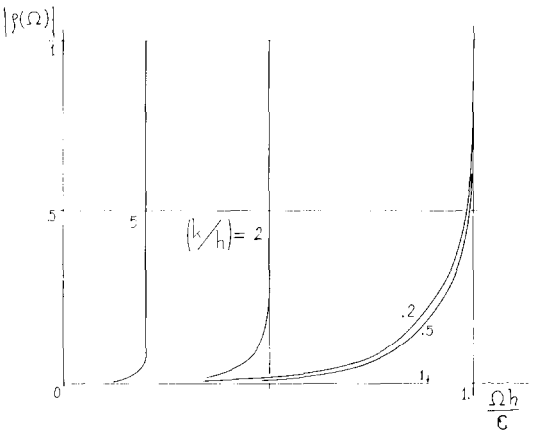

Fig. 8.

(instead of (4) used in the 'standard' procedure).

Fundamental solutions in both regions are, as before, expressed by the characteristic ratios (11), (14) and (19).

To analyse reflection in $x = 0$ we assume, as in the preceding case, that fundamental solutions of both types exist in $x < 0$:

$$\{u_n\} = \{p_n\} + \{q_n\}\,, \quad n < 0\,, \tag{58}$$

while only a fundamental solution of the first type (corresponding to positive group velocities) exist for $x > 0$:

$$\{u_n\} = \{r_n\}\,, \quad n > 0\,. \tag{59}$$

Near the origin, we have

$$u_{0,\mathrm{R}} = p_0 + q_0 \tag{60}$$

and

$$u_{0,\mathrm{L}} = r_0\,. \tag{61}$$

The expression of (56)–(57) in terms of Fourier transforms of the fundamental solutions is thus

$$\hat{r}_0(1+\hat{F}) = \hat{p}_0(\hat{E}_1^{-1}+1) + \hat{q}_0(\hat{E}_2^{-1}+1)$$

$$= \hat{p}_0(1-\hat{E}_2) + \hat{q}_0(1-\hat{E}_1)\,, \tag{62}$$

$$\hat{r}_0\left(\frac{\hat{F}-1}{k}\right) = \frac{\hat{p}_0(1-\hat{E}_1^{-1}) + \hat{q}_0(1-\hat{E}_2^{-1})}{h}$$

$$= \frac{\hat{p}_0(1+\hat{E}_2) + \hat{q}_0(1+\hat{E}_1)}{h}\,. \tag{63}$$

Eliminating $\hat{r}_0$ between these two relations and solving for $\rho(\Omega) \equiv \hat{q}_0/\hat{p}_0$ results in

$$\rho(\Omega) \equiv \frac{\hat{q}_0(\Omega)}{\hat{p}_0(\Omega)} = \frac{h(\hat{E}_2-1)(\hat{F}-1)+k(\hat{E}_2+1)(\hat{F}+1)}{h(\hat{E}_1-1)(\hat{F}-1)+k(\hat{E}_1+1)(\hat{F}+1)}$$

$$= \frac{\hat{E}_2}{\hat{E}_1}\,\frac{h(1+\hat{E}_1)(\hat{F}-1)+k(1-\hat{E}_1)(\hat{F}+1)}{h(1+\hat{E}_2)(\hat{F}-1)+k(1-\hat{E}_2)(\hat{F}+1)}\,. \tag{64}$$

This function is illustrated in Fig. 8.

10. Convergence rates for the modified scheme

To analyse the convergence rates, we expand as before (64) in Taylor series and find, for $h \to 0$ and k/h = constant

$$\rho = \frac{\mathrm{i}}{4}\left(\frac{\Omega}{c}\right)^3 h(k^2-h^2) + \cdots$$

$$= \mathrm{O}(h^3) \tag{65}$$

(to be compared with (50)).

Using this result to assess the convergence rate of the different components of the solution as we did in Section 8, we readily find that

– $\{p_n\}$ *approximates the exact solution in* $x > 0$ *with an error that converges to zero as* $\mathrm{O}(h^2)$

– $\{q_n\}$, *which is spurious, converges to zero as* $\mathrm{O}(h^3)$.

From (56), (60) and (61) we derive

$$\hat{r}_0 = \frac{\hat{p}_0(1+E_1^{-1}) + \rho\hat{p}_0(1+\hat{E}_2^{-1})}{1+\hat{F}}$$

$$= \hat{U}(0-\tfrac{1}{2}k, \Omega)(1+\mathrm{O}(h^2))\,. \tag{66}$$

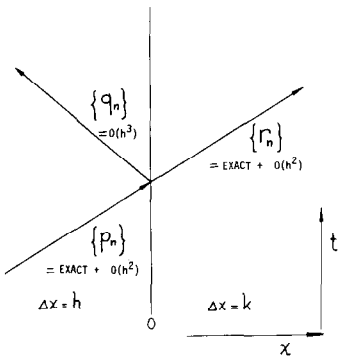

Fig. 9. Convergence rates for the different components of the numerical solution in the modified treatment of the interface point $x = 0$.

Proceeding as above we find that:
– $\{r_n\}$ *approximates the exact solution in* $x > 0$ *with an error that converges to zero as* $O(h^2)$.

While the reflection ratio, and the resulting amplitude of the spuriously reflected $\{q_n\}$, converge to zero as $O(h^3)$, we see that it is nevertheless the case that the global accuracy is only $O(h^2)$, here as it was for the standard case treated before. The only improvement is in a reduction of the amplitude of the reflected solution (Fig. 9).

11. Energy in the modified scheme

We have shown (Section 7) that the reflection ratio of the 'standard' treatment of the interface between two mesh sizes verified the principle of conservation of the total energy. Since (64) is different, one may suspect that energy is not conserved by the scheme described by equations (56)–(57). This, indeed, is found to be the case:

The discrete energy over the mesh defined by (60), using the same rectangular rule to approximate the continuous integral (5) is

$$\|u_n\|_2^2 = h \sum_{n<0} u_n^2 + k \sum_{n>0} u_n^2 . \tag{67}$$

Its time derivative is expressed by multiplying each equation in (2) by $2u_n h$ for $n < 0$, each equation in (3) by $2u_n k$ for $n > 0$ and summing over all $n \neq 0$:

$$\frac{d}{dt}\|u_n\|_2^2 = 2h \sum_{n<0} u_n \dot{u}_n + 2k \sum_{n>0} u_n \dot{u}_n$$
$$= c(-u_{-1}u_{0,R} + u_{0,L}u_1) . \tag{68}$$

(We have deleted those terms in $u_{\pm\infty}$ which vanish for $\{u_n\}$ in $\mathcal{L}_2$.) The expression for $u_{0,L}$ and $u_{0,R}$ is obtained by solving (56)–(57), resulting in

$$u_{0,L} = \frac{2u_{-1} + u_1(1 - h/k)}{1 + h/k} , \tag{69}$$

$$u_{0,R} = \frac{2u_1 - u_{-1}(1 - k/h)}{1 + k/h} . \tag{70}$$

Inserting in (73) results in

$$\frac{d}{dt}\|u_n\|_2^2 = c\left(\frac{h-k}{h+k}\right)(u_1 - u_{-1})^2 . \tag{71}$$

This expression does not vanish in general: the treatment (56)–(57) of the interface point does not conserve the global energy. As expected, though, (71) equals zero when there is no mesh variation ($h = k$) and when the solution near $x = 0$ is a constant ($u_1 = u_{-1}$).

Note also that the change of global energy cannot change sign: there is an *increase* of the total energy when any non-constant solution passes through the interface in *mesh refinement* ($h > k$) and a *decrease* in the total energy in *mesh coarsening* ($h < k$).

12. Comments

Some general comments on the tools used to derive the results of this paper are in order: If $\{p_n\}$ would consist of a solution at a single frequency Ω, then, by (20) and (21), $\{q_n\}$ and $\{r_n\}$ would also contain only the single frequency Ω. Thus, the frequency Ω is conserved when numerical solutions pass through the mesh discontinuity. *It is precisely this conservation of* Ω *through the discontinuity that makes t-Fourier transforms the appropriate tool for the analysis of this class of problems.*

By contrast, the space frequency ω that is used with x-Fourier transforms is not conserved across mesh discontinuities, and therefore, x-Fourier transforms cannot be used for those derivations.

But as a post-facto complement to an analysis of reflection that has been carried out with t-Fourier transforms, x-Fourier transforms are useful, as we have seen, in describing the various components of the solution and their energy.

References

[1] R. Vichnevetsky, Energy and group velocity in semi-discretizations of hyperbolic equations, Math. Comput. Simulation XXIII (1981) 333–343, this issue; *and all references cited therein.*

[2] G. Browning, H.-O. Kreiss and J. Oliger, Mesh refinement, Math. Comput. 27 (1973) 29–39.

[3] J.H. Chen and K. Miyakoda, A nested grid computation for the barotropic free surface atmosphere, Monthly Weather Rev. 102 (2) (1974) 181–190.

[4] B. Engquist and A. Majda, Absorbing boundary conditions for the simulation of waves, Math. Comput. 31 (139) (1977) 629–651.

[5] B. Gustafsson, The convergence rate for difference approximations to mixed initial boundary value problems, Math. Comput. 29 (1975) 396–406.

[6] E. Isaacson, Error estimates for parabolic equations, Comm. Pure Appl. Math. 14 (1961) 381–389.

[7] R. Vichnevetsky, Propagation characteristics of semi-discretization of hyperbolic equations, Math. Comput. Simulation XXII (1980) 98–107.